An Investigation of the Effect of Embedded Gold Nanoparticles in Different Geometric Shapes on the Directivity of THz Photoconductive Antennas

Yunus Emre Karasu
Faculty of Engineering, Karabuk University, Turkiye
yekarasu@karabuk.edu.tr (corresponding author)

Ihsan Uluer
Faculty of Engineering, Ostim Technical University, Turkiye
ihsanuluer@gmail.com

Turgut Ozturk
Faculty of Engineering, Karabuk University, Turkiye
t.ozturk@karabuk.edu.tr

Received: 11 June 2023 | Revised: 21 June 2023 | Accepted: 2 July 2023

 DOI: https://doi.org/10.48084/etasr.6116

ABSTRACT

This study aims to show how Terahertz (THz) Photoconductive Antennas (PCAs) affect the radiation directivity when gold nanoparticles of various geometric shapes are embedded in the gap region between the electrodes of THz PCAs. Three different PCAs, in the frequency range of 0.1 to 2 THz, conventional and after the addition of cylindrical, triangular, square, and hexagonal geometric gold nanoparticles to the antenna gap region between the electrodes, were built and simulated. The antenna directivity increased from 4.71 dBi to 4.92 dBi when square nanoparticles were added to the bowtie PCA, from 4.33 dBi to 4.45 dBi when triangular nanoparticles were added to the dipole PCA, and from 7.18 dBi to 7.52 dBi when square nanoparticles were added to the Vivaldi PCA.

Keywords-photoconductive antenna; terahertz waves; nanoparticles

I. INTRODUCTION

The THz gap is the area between far infrared (10 THz) and microwave rays (100 GHz) in the electromagnetic spectrum. THz rays have been used in a very important and wide range, from imaging for security purposes to food spectroscopy and from space communication to drug and explosive material detection [1]. Many devices can radiate at THz frequency. However, most are complex, expensive, inefficient, and cannot function at room temperature [2]. Until recently, there has been no progress in THz applications for these reasons. With the production of ultra-fast lasers, PCAs have become ideal devices that can be used as a source and detector for THz radiation and operate at room temperature [3, 4].

The PCA is obtained as follows: electrodes are added on top of the semiconductor substrate. A DC bias is applied to the electrodes. An optical pulse of a certain frequency is applied to the semiconductor material at a certain time interval. The energy of the applied optical radiation should be sufficient to transfer the electrons from the valence band of the semiconductor material to the conduction band. Electrons and holes emerge in the material when the semiconductor surface is illuminated with an optical laser. With DC bias, electrons and holes are aligned and accelerated. When the radiation ends, electrons and holes recombine and slow down. With the acceleration of electrons and holes, photocurrent occurs in the antenna gap. Due to the photocurrent's emergence and change, radiation occurs from the side of the substrate to space [5, 6]. With the enhancement of ultrafast pulsed lasers [4] and the development of low-temperature grown GaAs (LT-GaAs) [7] the use of PCAs as a room-temperature source and detector for THz radiation has become very common. According to the geometric shape of the THz PCA electrode, it can be divided into bowtie, Vivaldi, log spiral, and dipole. Semi-insulating GaAs (SI-GaAs), GaAs, LT-GaAs, Graphene, and Quartz were used as photoconductive materials [3, 8]. Enhancement of high power of THz radiation produced from PCAs or increasing optical-THz conversion efficiency is based on two principles:

The first is the change in the density of the photocarrier, and the second is the change in its velocity [9, 10]. Something that limits the increase in the photocarrier density in the PCA and thus reduces the power and directivity of the radiation is the phenomenon known as delay saturation or screening effect. To reduce the screening effect, conductive nanoparticles have been added to the gap between electrodes where the optical pulse is applied. Adding conductive nanoparticles increases the absorption of the ultrafast optical pulse, and a shorter lifetime photocarrier is obtained. To reduce the screening effect, the nanoparticles should not be placed on the gap in a three-dimensional manner but should be embedded in the gap [11]. The added nanoparticles should have high conductivity [12]. A part of the power used for radiation in the PCA is consumed in the substrate material. To overcome this problem, slots are opened on the antenna surface in order to reduce the surface wave loss and increase the optical-THz conversion ratio and directivity. When opening a slot, it is more efficient to open it in certain geometric shapes instead of a random shape [13, 14].

In this study, gold nanoparticles in certain geometric shapes were added to the antenna's gap to increase the PCA's directivity. The chosen geometric shapes of the added gold nanoparticles were as cylinder, triangle, square, and hexagon. As antenna type, studies were carried out on bowtie, dipole, and Vivaldi antennas. First, conventional antennas were analyzed in the CST MW Studio simulation program. Then, the geometric shapes were added, and the new PCAs were analyzed. With the addition of nanoparticles to the antennas, its directivity increased. The highest directivity was achieved in the bowtie and Vivaldi antennas when square-shaped particles were added. The highest directivity in the dipole antenna was achieved when triangular gold nanoparticles were added.

II. MATHEMATICAL MODEL OF THZ PCA

The current density $J(t)$ in the PCA gap is given as [13]:

$$J(t) = n(t).\ v(t) \cdot e \tag{1}$$

where $v(t) = E_b(t).\mu_e$ is the average velocity of the carrier, e is the electron charge, $E_b(t)$ is the electric field in the conductive antenna gap, μ_e is the electron mobility, and $n(t)$ is the time-dependent carrier density. The time-dependent carrier density is expressed using the Drude model [15]:

$$\frac{dn(t)}{dt} = -\frac{n(t)}{\tau_i} + \frac{\alpha_p}{\gamma \cdot h} I_p(t) \tag{2}$$

where γ is represented by laser frequency, optical absorption coefficient α_p, carrier lifetime τ_i, and peak laser intensity $I_p(t)$.

The electric field in the antenna gap is screened by the increase in the separation of charge carriers. The photoconductive substrate can be considered as a current source, dependent on the source resistance and time. The resistance depends on the optical source and substrate material and is also a time dependent variable, denoted as $R(t)$:

$$R(t) = \frac{1}{G(t)} \tag{3}$$

where $G(t)$ is the time-varying source conductivity, given by:

$$G = \frac{W_a,\mu,e}{L_a}\ (1 - e^{-\alpha T_s}) I_p\ \exp(-2)\,(1\ -R) \times \frac{\sqrt{2\pi}}{4hv} \mathrm{r}_p\ \exp\left(-\frac{r_p^2}{\tau_i}\right) \left(\mathrm{erf}\left(\frac{\sqrt{2}t}{\mathrm{r}_p}\right. \quad \left. -\frac{\sqrt{2}\mathrm{r}_p}{4\tau_i}\right)\right) + 1 \tag{4}$$

where W_a and L_a are the width and length of the antenna gap, respectively, α is the optical absorption coefficient, μ is the electron mobility, e is the electron charge, v is the frequency, h is the Planck constant, I_p is the peak laser intensity, T_s is the skin depth of the excitation region, r_p is the laser pulse duration, and R is the reflection coefficient of the substrate [16]. The voltage across the time-varying PCA range is given as follows:

$$\frac{dV_g(t)}{dt} = \frac{1}{Z_g\,C(t)} V_b - \frac{1}{Z_g\,C(t)} V_g(t) - \frac{\beta(t)}{Z_g\,C(t)} V_g(t) - \frac{G(t)}{C(t)} V_g(t) - \frac{1}{C(t)} \frac{dC(t)}{dt} \tag{5}$$

where V_b is the bias voltage and $C(t)$ is the time-dependent capacitance [17]:

$$C(t) = \frac{\tau_t}{Z_g}\left[1 + \frac{\mu \cdot e \cdot Z_g \cdot A \cdot n(t)}{L_d}\right] \tag{6}$$

where τ_t is the recombination time, A is the active area, and L_d is the dipole length of the antenna. The voltage-controlled time-dependent resource coefficient $\beta(t)$ depends on the recombination time and carrier density:

$$\beta(t) = \frac{\tau_t \mu \mathrm{en}(t)}{\varepsilon \zeta} \tag{7}$$

The produced photocurrent is given by:

$$i_p(t) = \mu \cdot e \cdot n(t) \cdot V_g(t) \cdot \frac{A}{L_d} \tag{8}$$

where $n(t)$ is the photocarrier density and $V_g(t)$ is the time-dependent voltage at the antenna gap [15].

III. THZ PCA DESIGN

A. Design of the Bowtie PCA

The parameters of the conventional bowtie PCA in Figure 1 without nanoparticles are shown in Table I. Gold was used as the electrode material. While designing the bowtie antenna, simulations were made in the CST MW Studio program using Quartz, GaAs, graphene, and LT-GaAs as substrates. The best S11 and directivity values were obtained when LT-GaAs was used as substrate. For this reason, LT-GaAs was used as the substrate material in this antenna. To increase the directivity of the conventional bowtie PCA, cylindrical, triangular, square, and hexagonal gold nanoparticles were added to the gap between the electrodes and simulated in the CST MW Studio. The highest directivity value was obtained in the bowtie PCA with square gold nanoparticles added. The bowtie antenna with square gold nanoparticles inserted between the electrodes can be seen in Figure 2. The side length of the gold square added in Figure 2(b) is 500 nm. The distances between the frames are equal and 500 nm. The nanoparticles of interest have been embedded in the substrate and have a depth of 10 nm. The return loss value (S11) of the PCA with bowtie antenna and square gold added nanoparticles is shown in Figure 3.

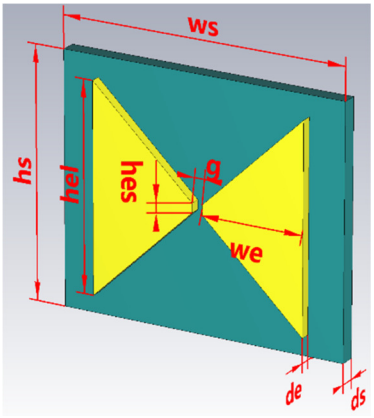

Fig. 1. Shape and parameters of conventional bowtie PCA.

TABLE I. PARAMETER VALUES OF CONVENTIONAL BOWTIE PCA

Parameter	Parameter Explanation	Value (μm)
ws	Substrate width	280
hs	Substrate height	240
ds	Substrate depth	1.5
hel	Height of the long side of the electrode	200
hes	Height of the short edge of the electrode	10
we	Width between the long edge and the short edge of the electrode	100
de	Depth of the electrode	0.01
g	Gap between electrodes	10
hes	Height of the short edge of the electrode	10

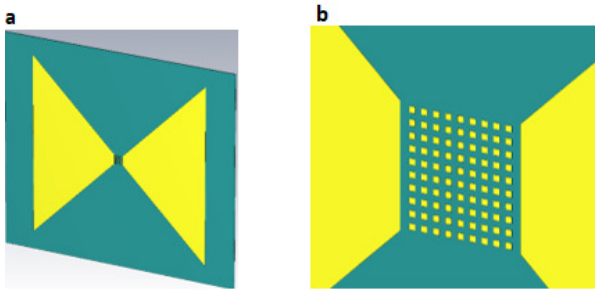

Fig. 2. (a) Zoomed-out view of bowtie PCA with added square nanoparticles. (b) Zoomed in view of the attached region of square-shaped gold nanoparticles between the electrodes.

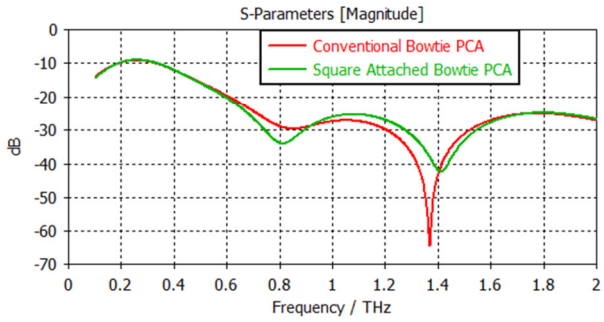

Fig. 3. Return loss information of conventional bowtie PCA and square attached bowtie PCA (S11).

As seen in Figure 3, when square nanoparticles are added to the conventional bowtie PCA, the S11 value increased from -64.5 dB to -42.27 dB, the bandwidth increased from 1.65 THz to 1.66 THz, and the resonant frequency increased from 1.36 THz to 1.41 THz. The directivity of the conventional bowtie PCA increased from 4.71 dBi to 4.92 dBi, as seen in Figure 4, whereas the directivity of the bowtie PCA with the addition of square gold nanoparticles can be seen in Figure 5.

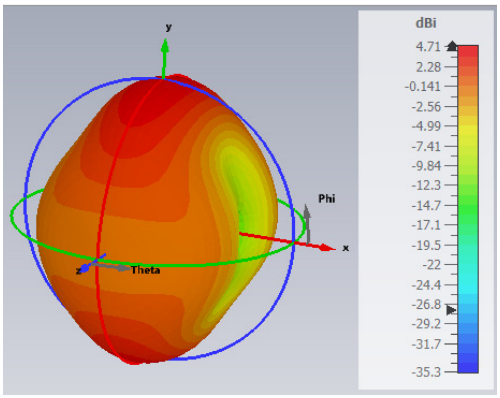

Fig. 4. 3D radiation patterns of conventional bowtie PCA.

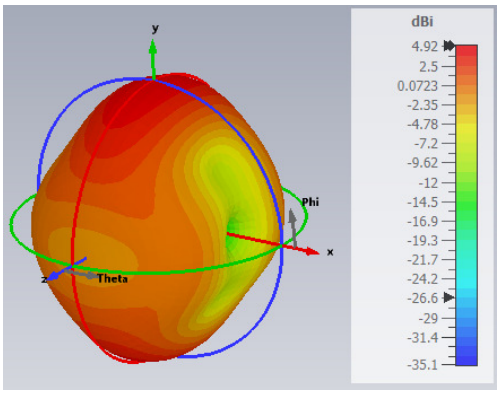

Fig. 5. 3D radiation patterns of square attached bowtie PCA.

B. Design of the Dipole PCA

The parameters of the conventional dipole PCA (Figure 1) without nanoparticles are shown in Table II. Gold was used as the electrode material. While designing the bowtie antenna, simulations were made in the CST MW Studio using Quartz, GaAs, Graphene, and LT-GaAs substrates. The best S11 and directivity value were obtained when GaAs was used, so GaAs was used as the substrate material in this antenna. To increase the directivity of the conventional dipole PCA, cylindrical, triangular, square, and hexagonal gold nanoparticles were added to the gap between the electrodes and were simulated in CST MW Studio. The highest directivity value was obtained in the dipole PCA with triangular gold nanoparticles added. The bowtie antenna with triangular gold nanoparticles inserted between the electrodes is shown in Figure 7. The side length of the gold triangular added in Figure 7 is 1 μm. The distances between the frames are equal and 500 nm. The nanoparticles of interest were embedded in the substrate and have a depth of 10 nm. The S11 of the conventional dipole PCA with triangular gold nanoparticles added is shown in Figure 8.

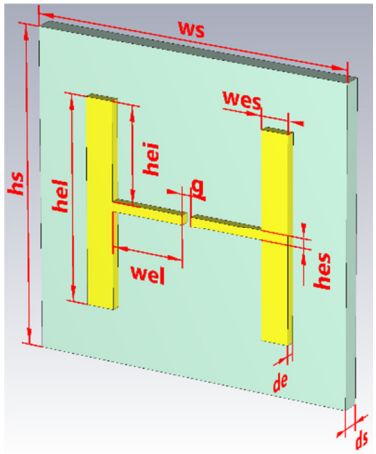

Fig. 6. Shape and parameters of conventional dipole PCA.

TABLE II. PARAMETER VALUES OF CONVENTIONAL DIPOLE PCA

Parameter	Parameter Explanation	Value (μm)
ws	Substrate width	350
hs	Substrate height	340
ds	Substrate depth	1.5
hel	Height of the long side of the electrode	220
hes	Height of the short edge of the electrode	10
wel	Width between the long edge and the short edge of the electrode	80
wes	Width of the long electrode	30
de	Depth of the electrode	0.02
g	Gap between electrodes	10

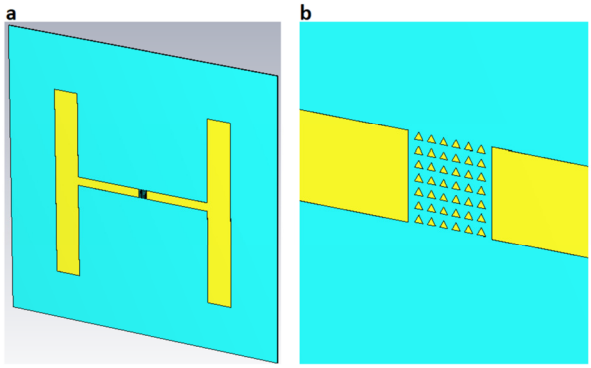

Fig. 7. a. Zoomed-out view of bowtie PCA with added triangular nanoparticles b. Zoomed in view of the attached gap of triangular -shaped gold nanoparticles between the electrodes

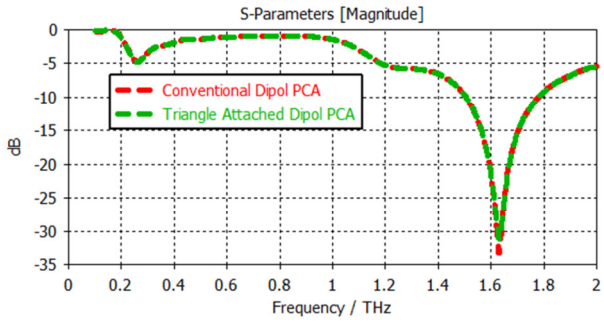

Fig. 8. S11 of conventional dipole PCA and triangular attached dipole PCA.

As can be seen in Figure 8, when triangular nanoparticles were added to the conventional dipole PCA, the S11 value increased from -33.27 dB to -31.2 dB, the bandwidth decreased from 0.28 THz to 0.27 THz, and the resonant frequency remained constant at 1.63 THz. The directivity of the conventional dipole PCA (Figure 9) increased from 4.33 dBi to 4.45 dBi. The directivity of the dipole PCA with the addition of triangular gold nanoparticles is shown in Figure 10.

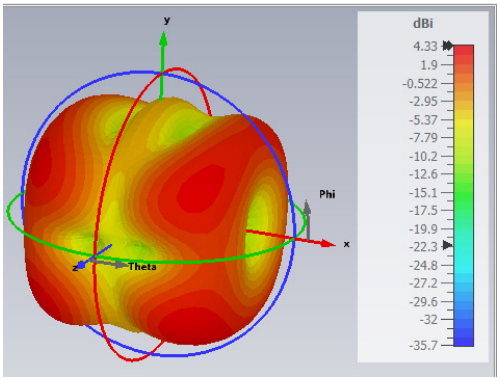

Fig. 9. 3D radiation patterns of conventional dipole PCA.

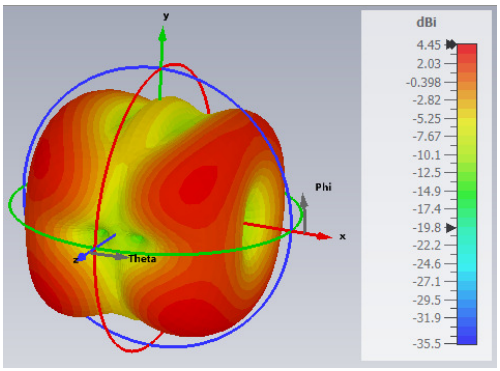

Fig. 10. 3D radiation patterns of triangular attached dipole PCA.

C. *Design of the Vivaldi PCA*

The parameters of the conventional Vivaldi PCA without nanoparticles in Figure 11 are shown in Table III. Gold was used as the electrode material. While designing the Vivaldi antenna, simulations were made in the CST MW Studio using Quartz, GaAs, graphene, and LT-GaAs as substrates. The best S11 and directivity values were obtained when GaAs was used as substrate, so GaAs was used as the substrate material in this antenna. To increase the directivity of the conventional Vivaldi PCA, cylindrical, triangular, square, and hexagonal gold nanoparticles were added to the gap between the electrodes and the structure was simulated in the CST MW Studio. The highest directivity value in the Vivaldi PCA was obtained with square gold nanoparticles added. The Vivaldi antenna with square gold nanoparticles inserted between the electrodes is shown in Figure 12. The side length of the gold square added in Figure 7 is 500 nm. The distances between the frames are equal and 500 nm. The nanoparticles used had a depth of 50 nm. The S11 of the conventional Vivaldi PCA and of the square gold added nanoparticles is shown in Figure 13.

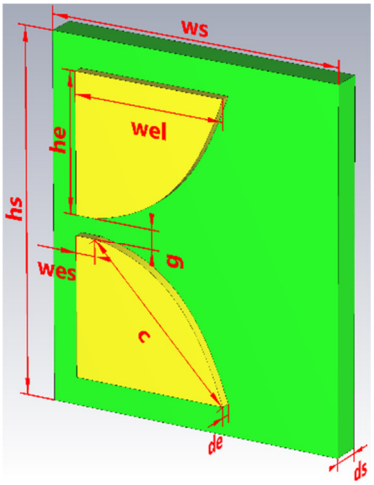

Fig. 11. Shape and parameters of conventional Vivaldi PCA.

TABLE III. PARAMETER VALUES OF THE CONVENTIONAL VIVALDI PCA

Parameter	Parameter Explanation	Value (μm)
ws	Substrate width	150
hs	Substrate height	180
ds	Substrate depth	1.5
he	Electrode height	69,4
wel	Width of the long side of the electrode	77.5
wes	Width of the short edge of the electrode	10
de	Depth of the electrode	0.05
g	gap between electrodes	10
c	Length of antenna curve	96.81

As seen in Figure 13, when square nanoparticles were added to the conventional Vivaldi PCA, The S11 value decreased from 32.08 dB to -31.2 dB, the bandwidth decreased from 0.28 THz to 0.27 THz, and the resonant frequency increased from 1.57 THz to 1.58 THz. The directivity of the conventional Vivaldi PCA (Figure 14) increased from 7.18 dBi to 7.52 dBi (Figure 15).

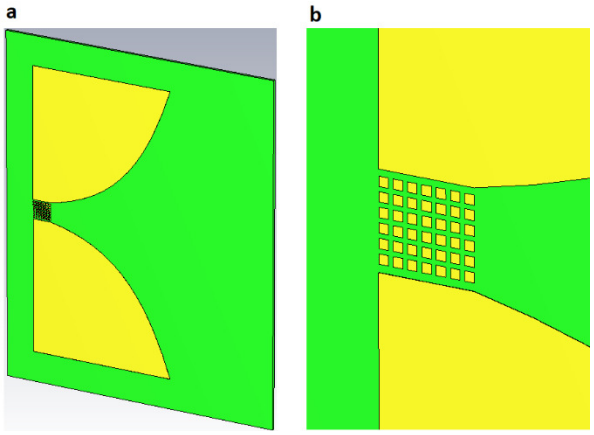

Fig. 12. (a) Zoomed-out view of the Vivaldi PCA with added triangular nanoparticles. (b) Zoomed in view of the attached gap of square -shaped gold nanoparticles between the electrodes.

The analysis results of all the studied PCAs, such as the substrate material used, the electrode material, the type of nanoparticle material added, the nanoparticle shape, S11, resonance frequency, bandwidth, and directivity are shown in Table IV. The electroded and the added nanoparticles are gold in all designs.

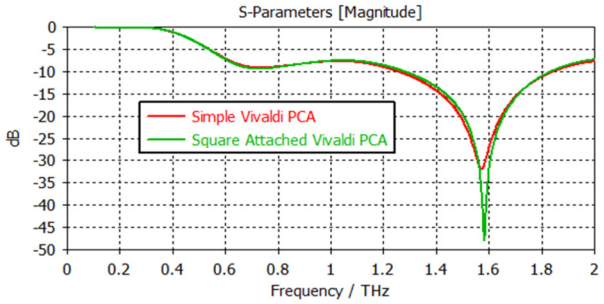

Fig. 13. S11 of conventional square attached Vivaldi PCAs.

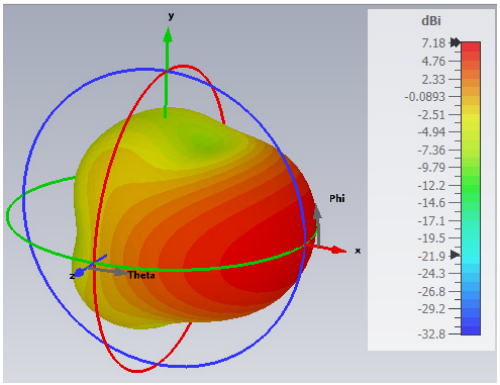

Fig. 14. 3D radiation patterns of conventional Vivaldi PCA.

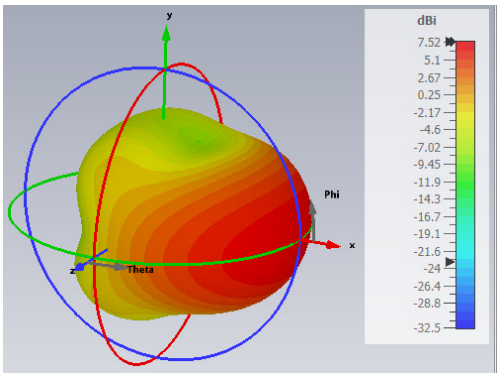

Fig. 15. 3D radiation patterns of square attached Vivaldi PCA.

IV. DISCUSSION

Various efforts have been made to increase the output power, optical to THz conversion ratio, and antenna directivity of the THz PCAs [13, 18]. The addition of metal nanoparticles to the photoconductive gap between the electrodes is one of these efforts [19, 21]. In this article, it has been shown that there is a relationship between the shape of the nanoparticle added to the photoconductive gap and the electrode shape of the antenna. In the bowtie and Vivaldi PCA, the highest directivity was reached when square-shaped nanoparticles were added, while in the dipole PCA, the highest directivity was reached when triangular-shaped nanoparticles were added.

TABLE IV. RESULT SUMMARY

PCA Type	Substrate used	Shape of the added nanoparticles	S11 (dB)	Bandwidth (THz)	Resonance frequency (THz)	Directivity (dBi)
Bowtie	LT-GaAs	No add	-64,5	1.65	1.36	4.71
Bowtie	LT-GaAs	Cylinder	-38,51	1.67	1.41	4.91
Bowtie	LT-GaAs	Triangle	-36,85	1.65	1.4	4.88
Bowtie	LT-GaAs	Square	-42,27	1.66	1.411	4.92
Bowtie	LT-GaAs	Hexagon	-45,9	1.66	1.40	4.88
Dipole	GaAs	No add	-33,27	0.28	1.631	4.33
Dipole	GaAs	Cylinder	-31,62	0.28	1.629	4.26
Dipole	GaAs	Triangle	-31,2	0.27	1.631	4.45
Dipole	GaAs	Square	-31,37	0.27	1.629	4.39
Dipole	GaAs	Hexagon	-33,55	0.27	1.625	4.37
Vivaldi	GaAs	No add	-32,08	0.58	1.572	7.18
Vivaldi	GaAs	Cylinder	-33,39	0.59	1.568	7.5
Vivaldi	GaAs	Triangle	-34,2	0.58	1.570	7.46
Vivaldi	GaAs	Square	-48,75	0.55	1.582	7.52
Vivaldi	GaAs	Hexagon	-38,02	0.55	1.576	7.41

Authors in [18] showed that plasmonic contact electrodes could significantly reduce photoconductive THz optoelectronics' low quantum efficiency performance. Authors in [12] further increased optical to THz conversion efficiency by adding silver nanoparticles to the gap between antenna electrodes. Authors in [19] proposed a photoconductive logarithmic spiral antenna with saw-toothed plasmonic contact electrodes to provide higher THz radiation than a conventional PCA. Authors in [20] showed that by integrating split-ring resonators like metallic structures into the coplanar lines of the PCA transmitter, the spectral characteristic of the generated THz radiation could be significantly manipulated. Author in [21] developed THz PCA arrays to increase their output power. Improved arrays were designed according to the crossfingers structure as a high-power THz generator. In these studies, nanoscale metal particles were added to the surface of the gap region of the PCA. However, they were not embedded in the substrate. In our study, gold nanoparticles were embedded in the substrate, reducing the screen effect formed in the substrate, resulting in more antenna directivity. Authors in [22] increased the radiation intensity by adding He+ ions to the semiconductor substrate in the PCA, increasing thus the radiation intensity up to a certain dose and decreasing it after a certain point. In this study, the He+ element was embedded in the substrate at the gap. However, embedding an element is quite difficult in the manufacturing process. In our study, embedding of metal nanoparticles into the substrate is easier thanks to the e-beam lithography [23].

Authors in [24] examined a photoconductive bowtie antenna with graphene electrodes on a photonic crystal substrate for THz radiation. The photonic crystal structure was formed by the periodic arrangement of cylindrical air holes in the Gallium Arsenide substrate to improve the performance of the basic antenna design. Authors in [13] studied photonic crystal substrates with cylindrical, square, triangular, and hexagonal shapes. It was shown that hexagonal-shaped photonic crystals provide the highest directivity and bandwidth, confirming their suitability for THz PCA. In the above mentioned studies, photocrystals in the form of an air gap were added to the antenna. Photocrystals in the antenna can cause the S11 value to increase. In our study, the addition of conductive nanoparticles instead of the air gap caused the PCA to work more effectively.

V. CONCLUSION

In this article, embedding different shaped nanoparticles to the substrate was proposed for increasing the directivity of THz PCAs. The proposed PCAs have been designed and their performance was analyzed and compared with the conventional PCAs. It was shown that the geometric shape of the embedded nanoparticles in the gap between the antenna electrodes caused different effects depending on the antenna type. Embedding nanoparticles in the antenna gap increased antenna directivity from 4.71 dBi to 4.92 dBi in bowtie PCA, from 4.33 dBi to 4.45 dBi in dipole PCA, and from 7.18 dBi to 7.52 dBi in Vivaldi PCA. The highest directivity was obtained when triangular gold nanoparticles were added to the dipole antenna and square gold nanoparticles were added to the bowtie and Vivaldi PCAs. In previous studies, nanoparticles were either added to the surface or inserted into the antenna gap with random shape. However, in this study, the nanoparticles were embedded in the gap and placed in the antenna gap with certain geometric shapes. For this reason, a more significant increment was established in antenna directivity. Our future work will aim to establish the THz PCAs manufacturing system and measure the radiated power of the proposed antennas.

REFERENCE LIST

[1] P. H. Siegel, "Terahertz technology," *IEEE Transactions on Microwave Theory and Techniques*, vol. 50, no. 3, pp. 910–928, 2002, https://doi.org/10.1109/22.989974.

[2] R. Köhler *et al.*, "Terahertz semiconductor-heterostructure laser," *Nature*, vol. 417, no. 6885, pp. 156–159, 2002, https://doi.org/10.1038/417156a.

[3] N. M. Burford and M. O. El-Shenawee, "Review of terahertz photoconductive antenna technology," *Oprical Engineering*, vol. 56, no. 1, Jan. 2017, https://doi.org/10.1117/1.OE.56.1.010901.

[4] M. Tani, K. Sakai, and H. Mimura, "Ultrafast photoconductive detectors based on semi-insulating GaAs and InP," *Japanese Journal of Applied Physics*, vol. 36, no. 9A,, Sep. 1997, Art. no. L117, https://doi.org/10.1143/JJAP.36.L1175.

[5] D. H. Auston, K. P. Cheung, and P. R. Smith, "Picosecond photoconducting Hertzian dipoles," *Applied Physics Letters*, vol. 45, no. 3, pp. 284–286, 1984, https://doi.org/10.1063/1.95174.

[6] S. K. Bitra and S. Miriyala, "An Ultra-Wideband Band Pass Filter using Metal Insulator Metal Waveguide for Nanoscale Applications," *Engineering, Technology & Applied Science Research*, vol. 11, no. 3, pp. 7247–7250, Jun. 2021, https://doi.org/10.48084/etasr.4194.

[7] M. Tani, S. Matsuura, K. Sakai, and S. Nakashima, "Emission characteristics of photoconductive antennas based on low-temperature-grown GaAs and semi-insulating GaAs," *Applied Optics*, vol. 36, no. 30, pp. 7853–7859, Oct. 1997, https://doi.org/10.1364/AO.36.007853.

[8] A. Yahyaoui *et al.*, "Design and comparative analysis of ultra-wideband and high directive antennas for THz applications," *Applied Computational Electromagnetics Society Journal*, vol. 36, no. 3, pp. 308–319, 2021, https://doi.org/10.47037/2020.ACES.J.360311.

[9] N. Khiabani, Y. Huang, Y.-C. Shen, and StephenJ. Boyes, "Theoretical Modeling of a Photoconductive Antenna in a Terahertz Pulsed System," *IEEE Transactions on Antennas and Propagation*, vol. 61, no. 4, pp. 1538–1546, 2013, https://doi.org/10.1109/TAP.2013.2239599.

[10] K. Mekki, O. Necibi, C. Boussetta, and A. Gharsallah, "Miniaturization of Circularly Polarized Patch Antenna for RFID Reader Applications," *Engineering, Technology & Applied Science Research*, vol. 10, no. 3, pp. 5655–5659, Jun. 2020, https://doi.org/10.48084/etasr.3445.

[11] L. Chen and H. Bagci, "Analysis of Screening Effects on Terahertz Photoconductive Devices Using a Fully-Coupled Multiphysics Approach," *Journal of Lightwave Technology*, vol. 39, no. 24, pp. 7876–7884, 2021, https://doi.org/10.1109/JLT.2021.3072890.

[12] S. Lepeshov *et al.*, "Boosting Terahertz Photoconductive Antenna Performance with Optimised Plasmonic Nanostructures," *Scientific Reports*, vol. 8, no. 1, Dec. 2018, Art. no. 6624, https://doi.org/10.1038/s41598-018-25013-7.

[13] M. Shalini and M. G. Madhan, "Theoretical investigations on the influence of photonic crystal shapes on the performance of graphene-based terahertz photoconductive bowtie dipole antenna," *Photonics and Nanostructures - Fundamentals and Applications*, vol. 51, 2022, Art. no. 101046, https://doi.org/https://doi.org/10.1016/j.photonics.2022.101046.

[14] T. Jadhav and S. Deshpande, "A Tri-band Planar Inverted-F Antenna with Complementary Split Ring Resonator and Reactive Impedance Surface for Wireless Application," *Engineering, Technology & Applied Science Research*, vol. 12, no. 1, pp. 7988–7992, Feb. 2022, https://doi.org/10.48084/etasr.4592.

[15] N. Khiabani, "Modelling, Design and Characterisation of Terahertz Photoconductive Antennas," Ph.D. dissertation, University of Liverpool, Liverpool, UK, 2013.

[16] P. F. Goldsmith, *Gaussian Beam, Quasioptical Propagation and Applications*. New York, NY, USA: IEEE Press, 1998.

[17] C. Sirtori, S. Dhillon, C. Faugeras, A. Vasanelli, and X. Marcadet, "Quantum cascade lasers: The semiconductor solution for lasers in the mid- and far-infrared spectral regions," *Physica Status Solidi (a)*, vol. 203, no. 14, pp. 3533–3537, Nov. 2006, https://doi.org/10.1002/pssa.200622389.

[18] C. W. Berry, N. Wang, M. R. Hashemi, M. Unlu, and M. Jarrahi, "Significant performance enhancement in photoconductive terahertz optoelectronics by incorporating plasmonic contact electrodes," *Nature Communications*, vol. 4, no. 1, Mar. 2013, Art. no. 1622, https://doi.org/10.1038/ncomms2638.

[19] X. Zhang, F. Zhan, X. Wei, W. He, and C. Ruan, "Performance Enhancement of Photoconductive Antenna Using Saw-Toothed Plasmonic Contact Electrodes," *Electronics*, vol. 10, no. 21, Jan. 2021, Art. no. 2693, https://doi.org/10.3390/electronics10212693.

[20] X. Shi *et al.*, "Photoconductive Meta-Antenna Enabling Terahertz Amplitude Spectrum Manipulation," *Advanced Photonics Research*, vol. 2, no. 1, 2021, Art. no. 2000036, https://doi.org/10.1002/adpr.202000036.

[21] F. Moradiannejad, "Improvement of terahertz photoconductive antennas array using crossfingers structure," *Journal of Computational Electronics*, vol. 20, pp. 922–927, 2021, https://doi.org/10.1007/s10825-021-01661-3.

[22] K. Yang *et al.*, "THz wave emission of GaAs induced by He+ ion implantation," *Nuclear Instruments and Methods in Physics Research Section B: Beam Interactions with Materials and Atoms*, vol. 307, pp. 199–202, Jul. 2013, https://doi.org/10.1016/J.NIMB.2013.01.085.

[23] A. Bhattacharya, D. Ghindani, and S. S. Prabhu, "Enhanced terahertz emission bandwidth from photoconductive antenna by manipulating carrier dynamics of semiconducting substrate with embedded plasmonic metasurface," *Optics Express*, vol. 27, no. 21, Oct. 2019, Art. no. 30272, https://doi.org/10.1364/oe.27.030272.

[24] M. Shalini and M. G. Madhan, "Photoconductive bowtie dipole antenna incorporating photonic crystal substrate for Terahertz radiation," *Optics Communications*, vol. 517, Aug. 2022, Art. no. 128327, https://doi.org/10.1016/J.OPTCOM.2022.128327.